Direct Measurement of Topological Numbers with Spins in Diamond

Fei Kong,[1] Chenyong Ju,[1,2,*] Ying Liu,[1] Chao Lei,[1,2] Mengqi Wang,[1] Xi Kong,[1,2] Pengfei Wang,[1,2] Pu Huang,[1,2] Zhaokai Li,[1,2] Fazhan Shi,[1,2] Liang Jiang,[3,†] and Jiangfeng Du[1,2,‡]

[1]*Key Laboratory of Microscale Magnetic Resonance and Department of Modern Physics, University of Science and Technology of China, Hefei 230026, China*

[2]*Synergetic Innovation Center of Quantum Information and Quantum Physics, University of Science and Technology of China, Hefei 230026, China*

[3]*Department of Applied Physics, Yale University, New Haven, Connecticut 06511, USA*

(Received 12 June 2016; published 4 August 2016)

Topological numbers can characterize the transition between different topological phases, which are not described by Landau's paradigm of symmetry breaking. Since the discovery of the quantum Hall effect, more topological phases have been theoretically predicted and experimentally verified. However, it is still an experimental challenge to directly measure the topological numbers of various predicted topological phases. In this Letter, we demonstrate quantum simulation of topological phase transition of a quantum wire (QW), by precisely modulating the Hamiltonian of a single nitrogen-vacancy (NV) center in diamond. Deploying a quantum algorithm of finding eigenvalues, we reliably extract both the dispersion relations and topological numbers. This method can be further generalized to simulate more complicated topological systems.

DOI: 10.1103/PhysRevLett.117.060503

Topological numbers were first introduced by Dirac to justify the quantization of electric charge [1], and later developed into a theory of magnetic monopoles as topological defects of a gauge field [2]. An amazing fact is that fundamental quantized entities may be deduced from a continuum theory [3]. Later on, topological numbers were used to characterize the quantum Hall effect [4,5] in terms of transition between topological phases [6]. Since the topological number in quantum Hall systems is directly proportional to the resistance in transport experiments, its robustness against local perturbations enables a practical standard for electrical resistance [4]. In the past few years, more topological materials have been discovered, including topological insulators [7,8], topological superconductors [9,10], etc.

Developing robust techniques to probe topological numbers becomes an active research topic of both fundamental and practical importance. Recently, a generalized method of extracting a topological number by integrating dynamic responses has been proposed [11]. Guided by this theoretical proposal, experiments have successfully measured the topological Chern number of different topological phases using superconducting circuits [12,13]. However, their measurement of the Chern number requires integration over continuous parameter space, which may not give an exactly discretized topological number. Different from the above integration approach, here we take the simulation approach [14–16] and use a single NV center in natural diamond at room temperature [17,18] to simulate a topological system. Moreover, we deploy a quantum algorithm of finding eigenvalues to map out the dispersion relations [19,20] and directly extract the topological number, which enables direct observation of the simulated topological phase transition.

We consider the topological phase transition associated with a semiconductor quantum wire with spin-orbital interaction, coupled to an s-wave superconductor and magnetic field [9,21–23]. At the boundary between different topological phases of the quantum wire, Majorana bound states can be created as a promising candidate for topological quantum information processing [24]. The Hamiltonian of this system can be described using the Nambu spinor basis $\psi^T = (\psi_\uparrow, \psi_\downarrow, \psi_\downarrow^\dagger, -\psi_\uparrow^\dagger)$:

$$H_{\mathrm{QW}} = p\sigma_z\tau_z + (p^2 - \mu)\tau_z + \Delta\tau_x + B_x\sigma_x, \qquad (1)$$

with the momentum p, chemical potential μ, pairing amplitude Δ, Zeeman energy B_x, and Pauli matrices σ_a and τ_a acting in the spin and particle-hole sectors, respectively. Without loss of generality, we may assume negative μ, non-negative B_x and Δ.

The system described by Eq. (1) has two different topological phases determined by the relative strength of $\{B_x, \mu, \Delta\}$: (i) the trivial superconductivity phase (denoted by SC phase) when $B_x < \sqrt{\Delta^2 + \mu^2}$, and (ii) the topological superconductivity phase (denoted by TP phase) when $B_x > \sqrt{\Delta^2 + \mu^2}$. The phase diagram and dispersion relations of different phases are illustrated in Fig. 1(a). There are four energy bands for this system, consisting of two particle bands and two hole bands. We may label the energy bands as 1, 2, 3, 4 from bottom to top as illustrated in Fig. 1(a). The gap between the 2nd and 3rd bands will disappear during the phase transition.

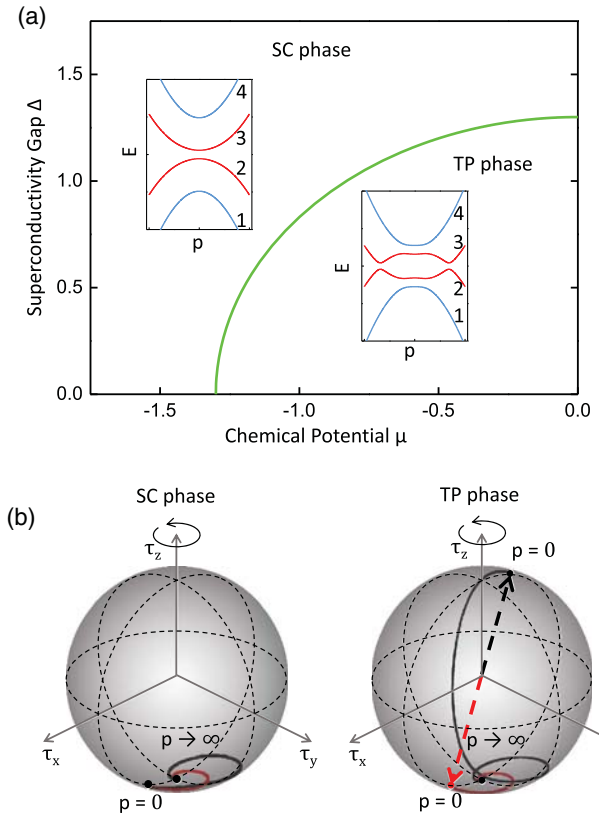

FIG. 1. Phase diagram and geometric illustration of the topologically distinct phases. (a) Phase diagram of quantum wire system (calculated at $B_x = 1.3$). The green line gives the boundary between the SC phase and TP phase. The energy dispersion relations of a SC point and a TP point are plotted in the insets. (b) Geometric illustration of the topological difference between the SC and the TP phases. In order to clearly visualize the two different trajectories associated with the 1st and 2nd energy eigenstates, the Bloch spheres are turned along the Z axis with p changes from 0 to ∞. This rotational transformation does not change the topological properties of the bitrajectories.

To illustrate the distinct topological nature associated with the SC and TP phases, we may consider the two lowest energy (i.e., 1st and 2nd) eigenstates with momentum p varying from 0 to ∞. First, it is easy to see that for $p \to \infty$, the second term (τ_z) in Eq. (1) dominates, which requires that the 1st and 2nd energy eigenstates be both eigenstates of τ_z with eigenvalue -1 [i.e., both pointing to the same direction of the Bloch sphere associated with τ, as illustrated in Fig. 1(b)]. For $p = 0$, $H_{\rm QW} = \sqrt{\mu^2 + \Delta^2}\tau_\phi + B_x\sigma_x$, where $\tau_\phi = (1/\sqrt{\mu^2 + \Delta^2})(-\mu\tau_z + \Delta\tau_x)$. The two lowest energy states are eigenstates of τ_ϕ with the same eigenvalue -1 (i.e., pointing in the same direction in the τ-Bloch sphere) when $\sqrt{\mu^2 + \Delta^2} > B_x$, or with different eigenvalues ± 1 (i.e., pointing in the opposite directions in the τ-Bloch sphere) when $\sqrt{\mu^2 + \Delta^2} < B_x$, as illustrated in Fig. 1(b). Hence, we may introduce the quantity $M(p) = \langle\vec{\tau}\rangle_1 \cdot \langle\vec{\tau}\rangle_2$ to characterize the alignment in the τ-Bloch sphere for the bitrajectories associated with two lowest energy eigenstates with momentum p, with $\langle\vec{\tau}\rangle_j = \langle\psi_j|\vec{\tau}|\psi_j\rangle$ for the jth lowest energy eigenstate $|\psi_j\rangle$. The two types of topologically different bitrajectories [with $M(p=0)\cdot M(p\to\infty) = \pm 1$] imply the existence of distinct topological phases for the system [25]. Mathematically, a topological number can be computed as the sign product of the Pfaffian of anti-symmetric matrices associated with momentum $p = 0$ and $p \to \infty$ [25]:

$$\nu = \mathrm{sgn}(\mu^2 + \Delta^2 - B_x^2). \tag{2}$$

Since $B_x + \sqrt{\mu^2 + \Delta^2}$ is always positive, the value of ν is determined by the sign of the quantity $-B_x + \sqrt{\mu^2 + \Delta^2}$, which is one of the eigenenergies of $H_{\rm QW}(p = 0)$. The corresponding eigenstate can be represented by $|\Phi\rangle = |\Phi_\sigma\rangle \otimes |\Phi_\tau\rangle$, where $|\Phi_\sigma\rangle$ and $|\Phi_\tau\rangle$ are the eigenstates of $B_x\sigma_x$ and $-\mu\tau_z + \Delta\tau_x$ with eigenenergies $-B_x$ and $\sqrt{\mu^2 + \Delta^2}$, respectively. It is direct to deduce $|\Phi_\sigma\rangle = |\leftarrow\rangle = (|\uparrow\rangle - |\downarrow\rangle)/\sqrt{2}$ ($|\uparrow\rangle$ and $|\downarrow\rangle$ means spin up and down) and $|\Phi_\tau\rangle = \alpha|p\rangle + \beta|h\rangle$ ($|p\rangle$ and $|h\rangle$ means particle and hole) which is dominated by $|p\rangle$ (i.e., $|\alpha|^2 > |\beta|^2$). Therefore, we can apply the quantum algorithm of finding eigenvalues [20] for the state $|\Phi\rangle$ to directly obtain the eigenenergy $-B_x + \sqrt{\mu^2 + \Delta^2}$, the sign of which is exactly the topological number ν.

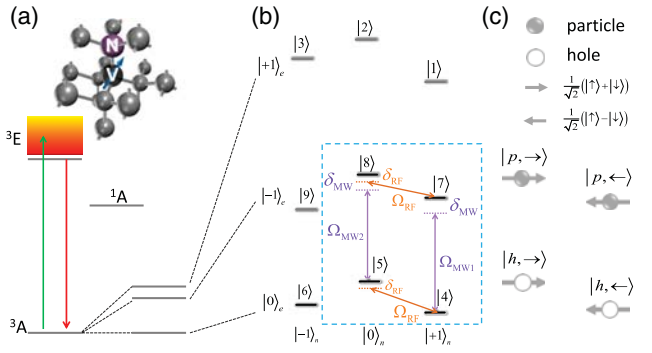

FIG. 2. NV system and its correlation with the QW system. (a) Structure and energy levels of the NV centers. (b) Hyperfine structure of the coupling system with NV electron spin and ^{14}N nuclear spin. The 9 energy levels are labeled as $|1\rangle$ to $|9\rangle$. The quantum simulation is carried out in the subspace spanned by $\{|4\rangle, |5\rangle, |7\rangle, |8\rangle\}$. Two MW pulses (purple arrows) and two RF pulses (orange arrows) are applied simultaneously to selectively drive the corresponding electron and nuclear spin transitions. (c) Four basis states of the QW system corresponding to the four NV states inside the square box.

The QW Hamiltonian is simulated by a highly controllable two-qubit solid-state system, which is a color defect named the NV center in diamond consisting of a substitutional nitrogen atom and an adjacent vacancy, as shown in Fig. 2(a). The electrons around the defect form an effective electron spin with a spin triplet ground state ($S = 1$)

and couple with the nearby ^{14}N nuclear spin. With an external magnetic field B_0 along the NV axis, the Hamiltonian of the NV system is ($\hbar = 1$) [31]:

$$H_{\mathrm{NV}}^{0} = -\gamma_e B_0 S_z - \gamma_n B_0 I_z + D S_z^2 + Q I_z^2 + A S_z I_z, \quad (3)$$

where S_z and I_z are the spin operators of the electron spin (spin-1) and the ^{14}N nuclear spin (spin-1), respectively. The electron and nuclear spins have gyromagnetic ratios $\gamma_e/2\pi = -28.03$ GHz/T and $\gamma_n/2\pi = 3.077$ MHz/T, respectively. $D/2\pi = 2.87$ GHz is the axial zero-field splitting parameter for the electron spin, $Q/2\pi = -4.945$ MHz is the quadrupole splitting of the ^{14}N nuclear spin, and $A/2\pi = -2.16$ MHz is the hyperfine coupling constant. There are nine energy levels, $|1\rangle, \ldots, |9\rangle$, as labeled in Fig. 2(b). The simulation is performed in the subspace spanned by $\{|4\rangle, |5\rangle, |7\rangle, |8\rangle\}$, associated with the electron spin states $\{m_{\mathrm{e}} = 0, -1\}$ (encoding the pseudospin σ) and the nuclear spin states $\{m_{\mathrm{n}} = 0, 1\}$ (encoding the pseudospin τ). The NV spins are radiated by two microwave (MW) pulses and two radio-frequency (RF) pulses simultaneously, which selectively drive the two electron-spin transitions and the two nuclear-spin transitions, respectively, as illustrated in Fig. 2(b). The frequencies of the pulses are all slightly detuned from resonance with detuning δ_{MW} for the two MW pulses and δ_{RF} for the two RF pulses. In the rotating frame, the Hamiltonian can be written as [25]

$$H_{\mathrm{NV}}^{\mathrm{rot}} = \frac{\Omega_{\mathrm{MW1}} - \Omega_{\mathrm{MW2}}}{4}\sigma_x\tau_z - \frac{1}{2}\delta_{\mathrm{RF}}\tau_z + \frac{\Omega_{\mathrm{MW1}} + \Omega_{\mathrm{MW2}}}{4}\sigma_x + \frac{\Omega_{\mathrm{RF}}}{2}\tau_x - \frac{1}{2}\delta_{\mathrm{MW}}\sigma_z, \quad (4)$$

where $\Omega_{\mathrm{MW1,2}}$ are the Rabi frequencies of the two electron spin transitions, Ω_{RF} is Rabi frequency of the two nuclear spin transitions that are set to the same value. By choosing $\Omega_{\mathrm{MW1}} = -\Omega_{\mathrm{MW2}} = \Omega_{\mathrm{MW}}$, the parameters for the QW system and the NV spins can be identified as the following: $p \sim \Omega_{\mathrm{MW}}/2$, $p^2 - \mu \sim -\delta_{\mathrm{RF}}/2$, $\Delta \sim \Omega_{\mathrm{RF}/2}$, and $B_x \sim -\delta_{\mathrm{MW}}/2$. Here, the numerical values of the left side are reduced by a factor of 11 to coincide with the typical values of NV parameters. Hence, H_{QW} can be exactly reproduced up to a Hadamard gate on the electron spin transforming the spin operators $\sigma_x \leftrightarrow \sigma_z$ in $H_{\mathrm{NV}}^{\mathrm{rot}}$. The Hadamard gate does not change the eigenvalues and can be fully compensated by modifying the basis states in the experiment. As shown in Fig. 2(c), the four states of the NV system can be mapped to a QW system one to one.

To obtain the energy-dispersion relations of QW and the topological number, we deploy a quantum algorithm of finding eigenvalues [20] to measure the eigenvalues of QW. The initial state of the NV spins is prepared to $(|6\rangle + |\Psi\rangle)/\sqrt{2}$, where $|6\rangle$ is used as a reference state and $|\Psi\rangle = |4\rangle, |5\rangle, |7\rangle$, or $|8\rangle$. In general, $|\Psi\rangle$ can be expanded by the QW eigenstates $|\Psi\rangle = \sum_{j=1}^{4} c_{\psi,j}|\phi_j\rangle$ ($H_{\mathrm{QW}}|\phi_j\rangle = E_j|\phi_j\rangle$). By applying the simulating pulses for an adjustable period $m\tau$ ($m \in \mathbb{N}$), $|\Psi\rangle$ evolves under the effective QW Hamiltonian and accumulates phases $\propto E_j m\tau$ with the state becoming $(|6\rangle + \sum_{j=1}^{4} c_{\psi,j} e^{-i2\pi E_j m\tau}|\phi_j\rangle)/\sqrt{2}$. It can be transformed back into the representation of NV spin states ($|\phi_j\rangle = \sum_{l=4,5,7,8} c_{l,j}^{*}|l\rangle$) and can be written as $(|6\rangle + \sum_{l=4,5,7,8} a_{l,m}|l\rangle)/\sqrt{2}$, with coefficients $a_{l,m} = \sum_{j=1}^{4} c_{\psi,j} c_{l,j}^{*} e^{-i2\pi E_j m\tau}$ which is a function of the QW eigenvalues. The coefficient of $|\Psi\rangle$, i.e., $a_{\psi,m}$, can be measured in the experiment. Therefore, the energy spectrum of the QW Hamiltonian can be obtained by Fourier transforming of the time-domain signals $\{a_{\psi,m}\}$. There will be at most four peaks in the energy spectrum with their heights $\propto |c_{\psi,j}|^2$. Since the 1st and 4th energy bonds are trivial, we only care about the 2nd and 3rd energy bonds. As $|c_{5(7),2}|^2 + |c_{5(7),3}|^2 \gg |c_{4(8),2}|^2 + |c_{4(8),3}|^2$ in the case of low momentum $|p| \ll \infty$ [25], $|\Psi\rangle$ is chosen to be $|5\rangle$ or $|7\rangle$ in the experiment. However, the detection of $\{a_{4,m}\}$ is easier than that of $\{a_{7,m}\}$. By reversing the sign of δ_{MW} and σ_z simultaneously in Eq. (4), one can see that the Hamiltonian remains unchanged. It means $|\Psi\rangle$ can choose $|4\rangle$ instead of $|7\rangle$ by using $\delta'_{\mathrm{MW}} = -\delta_{\mathrm{MW}}$.

The experimental realization was preformed on a home-built setup which has been described earlier [32]. The external statistical magnetic field was adjusted around 50 mT in order to polarize the ^{14}N nuclear spin using dynamic polarization technology [33]. The experimental process is shown in Fig. 3(a). At first, the NV system was prepared to $|4\rangle$ by a 4 μs laser pulse, then transformed to the superposition state $(|6\rangle + |\Psi\rangle)/\sqrt{2}$ during the initialization process. ($|\Psi\rangle = |5\rangle$ by the second row RF pulses and $|\Psi\rangle = |4\rangle$ by the third row RF pulses shown in the brackets). After that, the two RF pulses and the two MW pulses for simulating the QW Hamiltonian were applied simultaneously with time length $m\tau$. Finally, the state was rotated back to $|4\rangle$ with phase shift θ and the photoluminescence was detected. As shown in Fig. 3(b), increasing the θ would lead to oscillating photoluminescence. $a_{\psi,m}$ could be obtained from the oscillation amplitude and phase [25]. With different pulse length $m\tau$, we observed the time-domain evolution of $a_{\psi,m}$ [see Fig. 3(c)]. The eigenvalue of the simulated Hamiltonian can be acquired by the Fourier transform of this time-domain signal [Fig. 3(d)].

Figure 4(a) shows the energy dispersion relations obtained in experiment for the two SC points ($\mu = -1.6$, -1.44), two TP points ($\mu = -1.14$, -0.98), and the critical point ($\mu = -1.29$), given $\Delta = 0.165$ and $B_x = 1.3$. The experimental results agree well with the theoretical expectations except for the TP points. The small energy gap in TP phase disappears due to the fluctuating magnetic field from the surrounding ^{13}C spin bath, which induces phase errors on the NV electron spin. The phase errors will cause not only peak broadening but also peak shifting on the energy

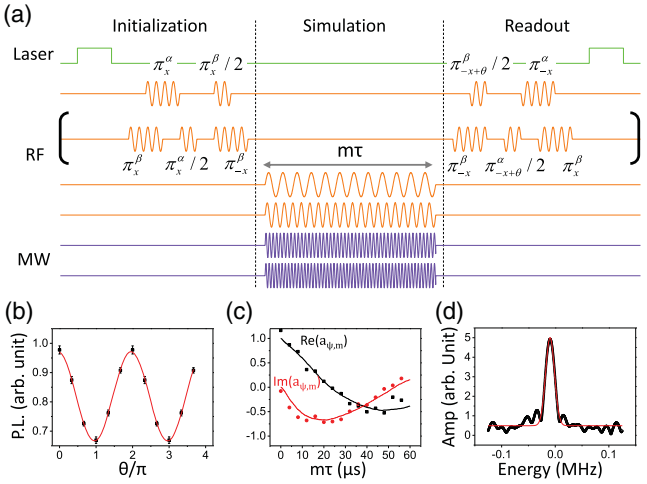

FIG. 3. Simulation of the QW Hamiltonian and detection of its eigenvalues. (a) The pulse scheme. The superscript $\alpha(\beta)$ of the RF pulses indicates the nuclear spin operation between $|4\rangle$ and $|5\rangle(|5\rangle$ and $|6\rangle)$. For the initialization and readout parts there are two pulse sequences, which correspond to the two initial state cases $|\Psi\rangle = |5\rangle$ (the upper pulse sequence) and $|4\rangle$ (the lower bracketed pulse sequence), respectively. (b) Photoluminescence (PL) changes versus different the RF $\pi/2$ pulse phase θ for fixed evolution time $m\tau$. The points are the experimental data and the curve is the sine function fit. Error bars indicate ± 1 standard deviation induced by the photon shot noise. (c) Measurement of $a_{\psi,m}$ with different evolution time $m\tau$. Black and red lines are the numerical calculation results. (d) The energy spectrum of the simulated Hamiltonian yielded from the Fourier transform of the time-domain data in (c). A Gaussian fit (the curve) is performed to get the exact eigenenergy value.

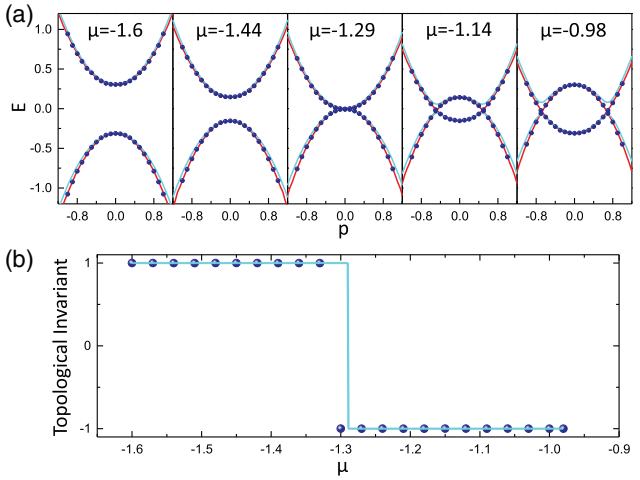

FIG. 4. Energy dispersion relations and topological phase transition. (a) Energy dispersion relations with different chemical potential μ. The points, light cyan lines, and red lines represent the experimental, analytical, and numerical results, respectively. Error bars given by fit error are smaller than the symbols. As the energy bonds are symmetrical about $p = 0$, only the right half points (i.e., $p \geq 0$) are actually measured in the experiment. (b) The measured topological number ν versus the chemical potential μ, which shows a topological phase transition happened near $\mu \approx -1.3$. The cyan line is the theoretical prediction.

spectrum [25]. In addition, the pulses applied are not perfectly selective pulses, the crosstalk between these pulses will also cause slight peak shifts on the energy spectrum [25]. The red lines in Fig. 4(a) give the numerical calculated energy dispersion including these imperfections which nicely coincide with the experimental results [25]. Further numerical simulation suggests that the energy gap can be observed if a NV sample with longer electron spin coherence time is adopted [25,34].

Even though the small energy gap of the TP phase is difficult to resolve at the current experimental condition, the topological number ν characterizing different topological phases can still be unambiguously extracted. As mentioned earlier, ν can be directly determined by the sign of the eigenenergy of $|\Phi\rangle$. Since $|\Phi\rangle$ is dominated by $|p, \leftarrow\rangle$ which is corresponding to $|7\rangle$ [see Figs. 2(b), 2(c)], the eigenenergy of $|\Phi\rangle$ can be reliably obtained from $\{a_{4,m}\}$. The sign of the eigenenergy can be calculated as

$$\overline{\mathrm{sgn}(E)} = \int_{-\infty}^{+\infty} \mathrm{sgn}(E) p(E) dE = \int_{-\infty}^{+\infty} \frac{\mathrm{sgn}(E)}{\sqrt{2\pi}\sigma} e^{-[(E-E_c)^2/2\sigma^2]} dE, \quad (5)$$

where E_c and σ are the fit center and the fit error of the energy spectrum [see Fig. 3(d)]. Figure 4(b) gives a clear illustration of the topological phase transition by measuring ν versus μ, where a sharp change of ν occurs near $\mu \approx -1.3$. The deviation of the critical point from the theoretical expectation value $\mu = -1.29$ is due to the inaccuracy of measuring the very small eigenenergy (close to 0) near the critical point for which even a slight shift will change its sign. This deviation can be eliminated by using a NV sample with longer coherence time [25]. Away from the critical point, the measured topological number will only have a negligibly small deviation from the exact value.

In conclusion, we have demonstrated quantum simulation of a topological phase transition with a single NV center at room temperature. Using a quantum algorithm of finding eigenvalues, we can not only obtain the dispersion relations, but also directly extract the topological number of the system. Different from the scheme of integration of dynamic responses [11–13], our approach of direct measurement of the topological number can unambiguously give a discretized value of ν over almost all parameter space except for a small region around the phase transition. Even in the presence of large magnetic field fluctuations that may smear out the energy gap in the dispersion relations, the approach of direct extraction of the topological number remains robust and unambiguously characterizes the topological phase transition.

We may further improve our NV-center-based quantum simulators by using isotopically purified diamond, with

significantly extended electron spin coherence time [34]. Moreover, with reliable control of multiple spins of the NV center [35], more complicated topological systems can be simulated. Utilizing entanglement can lead to a scalable quantum simulator of NV centers [36]. In addition, the quantum algorithm of finding eigenvalues can be extremely efficient for multiple spins, with only a polynomial time overhead with the number of spins [20]. Therefore, the NV-center-based quantum simulator is a very promising platform, which will provide a powerful tool to investigate novel quantum systems.

This work was supported by the National Key Basic Research Program of China (Grant No. 2013CB921800), the National Natural Science Foundation of China (Grants No. 11227901, No. 91021005, No. 11104262, No. 31470 835), and the Strategic Priority Research Program (B) of the CAS (Grant No. XDB01030400). L. J. acknowledges the support from ARL-CDQI, ARO (Grants No. W911NF-14-1-0011, No. W911NF-14-1-0563), AFOSR MURI (Grants No. FA9550-14-1-0052, No. FA9550-14-1-0015), Alfred P. Sloan Foundation (Grant No. BR2013-049), the Packard Foundation (Grant No. 2013-39273).

*cyju@ustc.edu.cn
†liang.jiang@yale.edu
‡djf@ustc.edu.cn

[1] P. A. M. Dirac, Proc. R. Soc. A **133**, 60 (1931).
[2] P. A. M. Dirac, Phys. Rev. **74**, 817 (1948).
[3] D. Thouless, *Topological Quantum Numbers in Nonrelativistic Physics* (World Scientific, Singapore, 1998).
[4] K. v. Klitzing, G. Dorda, and M. Pepper, Phys. Rev. Lett. **45**, 494 (1980).
[5] H. L. Stormer, D. C. Tsui, and A. C. Gossard, Rev. Mod. Phys. **71**, S298 (1999).
[6] X. G. Wen, Int. J. Mod. Phys. B **04**, 239 (1990).
[7] X.-L. Qi and S.-C. Zhang, Rev. Mod. Phys. **83**, 1057 (2011).
[8] M. Z. Hasan and C. L. Kane, Rev. Mod. Phys. **82**, 3045 (2010).
[9] J. Alicea, Rep. Prog. Phys. **75**, 076501 (2012).
[10] C. W. J. Beenakker, Rev. Mod. Phys. **87**, 1037 (2015).
[11] V. Gritsev and A. Polkovnikov, Proc. Natl. Acad. Sci. U.S.A. **109**, 6457 (2012).
[12] M. D. Schroer, M. H. Kolodrubetz, W. F. Kindel, M. Sandberg, J. Gao, M. R. Vissers, D. P. Pappas, A. Polkovnikov, and K. W. Lehnert, Phys. Rev. Lett. **113**, 050402 (2014).
[13] P. Roushan, C. Neill, Y. Chen, M. Kolodrubetz, C. Quintana, N. Leung, M. Fang, R. Barends, B. Campbell, Z. Chen *et al.*, Nature (London) **515**, 241 (2014).
[14] R. P. Feynman, Int. J. Theor. Phys. **21**, 467 (1982).
[15] S. Lloyd, Science **273**, 1073 (1996).
[16] I. M. Georgescu, S. Ashhab, and F. Nori, Rev. Mod. Phys. **86**, 153 (2014).
[17] A. Gruber, A. Dräbenstedt, C. Tietz, L. Fleury, J. Wrachtrup, and C. von Borczyskowski, Science **276**, 2012 (1997).
[18] P. C. Maurer, G. Kucsko, C. Latta, L. Jiang, N. Y. Yao, S. D. Bennett, F. Pastawski, D. Hunger, N. Chisholm, M. Markham, D. J. Twitchen, J. I. Cirac, and M. D. Lukin, Science **336**, 1283 (2012).
[19] C. Ju, C. Lei, X. Xu, D. Culcer, Z. Zhang, and J. Du, Phys. Rev. B **89**, 045432 (2014).
[20] D. S. Abrams and S. Lloyd, Phys. Rev. Lett. **83**, 5162 (1999).
[21] Y. Oreg, G. Refael, and F. von Oppen, Phys. Rev. Lett. **105**, 177002 (2010).
[22] R. M. Lutchyn, J. D. Sau, and S. Das Sarma, Phys. Rev. Lett. **105**, 077001 (2010).
[23] L. Jiang, D. Pekker, J. Alicea, G. Refael, Y. Oreg, A. Brataas, and F. von Oppen, Phys. Rev. B **87**, 075438 (2013).
[24] J. Alicea, Y. Oreg, G. Refael, F. von Oppen, and M. P. A. Fisher, Nat. Phys. **7**, 412 (2011).
[25] See Supplemental Material at http://link.aps.org/supplemental/10.1103/PhysRevLett.117.060503 for detailed discussion on the topological phases, topological numbers, quantum simulation and numerical calculation, which includes Refs. [26–30].
[26] A. Y. Kitaev, Phys. Usp. **44**, 131 (2001).
[27] L. Childress, M. V. Gurudev Dutt, J. M. Taylor, A. S. Zibrov, F. Jelezko, J. Wrachtrup, P. R. Hemmer, and M. D. Lukin, Science **314**, 281 (2006).
[28] B. Smeltzer, J. McIntyre, and L. Childress, Phys. Rev. A **80**, 050302 (2009).
[29] S. Felton, A. M. Edmonds, M. E. Newton, P. M. Martineau, D. Fisher, D. J. Twitchen, and J. M. Baker, Phys. Rev. B **79**, 075203 (2009).
[30] M. Leskes, P. Madhu, and S. Vega, Prog. Nucl. Magn. Reson. Spectrosc. **57**, 345 (2010).
[31] J. H. N. Loubser and J. A. van Wyk, Rep. Prog. Phys. **41**, 1201 (1978).
[32] F. Shi, X. Kong, P. Wang, F. Kong, N. Zhao, R. Liu, and J. Du, Nat. Phys. **10**, 21 (2014).
[33] V. Jacques, P. Neumann, J. Beck, M. Markham, D. Twitchen, J. Meijer, F. Kaiser, G. Balasubramanian, F. Jelezko, and J. Wrachtrup, Phys. Rev. Lett. **102**, 057403 (2009).
[34] G. Balasubramanian, P. Neumann, D. Twitchen, M. Markham, R. Kolesov, N. Mizuochi, J. Isoya, J. Achard, J. Beck, J. Tissler, V. Jacques, P. R. Hemmer, F. Jelezko, and J. Wrachtrup, Nat. Mater. **8**, 383 (2009).
[35] C. Bonato, M. S. Blok, H. T. Dinani, D. W. Berry, M. L. Markham, D. J. Twitchen, and R. Hanson, Nat. Nanotechnol. **11**, 247 (2015).
[36] N. Y. Yao, L. Jiang, A. V. Gorshkov, P. C. Maurer, G. Giedke, J. I. Cirac, and M. D. Lukin, Nat. Commun. **3**, 800 (2012).